

Detailed Analysis of the Chiral Unitary Model for Meson-Baryon Scattering with Flavor $SU(3)$ Breaking Effects

Tetsuo HYODO¹, Seung-il NAM^{1,2}, Daisuke JIDO^{1,*} and Atsushi HOSAKA¹

¹*Research Center for Nuclear Physics (RCNP), Ibaraki, 567-0047, Japan*

²*Department of Physics, Pusan National University, Pusan 609-735, Korea*

We study s -wave meson-baryon scattering using the chiral unitary model. We consider $1/2^-$ baryon resonances as quasibound states of the low lying mesons (π, K, η) and baryons (N, Λ, Σ, Ξ). In previous works, the subtraction constants which appear in loop integrals were found to largely depend on the channels, and it was necessary to fit these constants to reproduce the data. In order to extend this model to all channels with fewer parameters, we introduce flavor $SU(3)$ breaking interactions in the framework of chiral perturbation theory. It is found, however, that the observed $SU(3)$ breaking in meson-baryon scattering cannot be explained by the present $SU(3)$ breaking interactions. The role and importance of the subtraction constants in the present framework are discussed.

§1. Introduction

A unified study of meson-baryon scattering in various channels is important to understand hadron dynamics in low and intermediate energy regions from the viewpoint of QCD. In particular, the properties of excited states of baryons observed in meson-baryon scattering as resonances have been investigated with great interest both theoretically and experimentally. At this time, there are several established approaches to describe the properties of baryon resonances. A recent development in this field is the introduction of the chiral unitary model,^{1),2),3),4),5),6)} in which the s -wave baryon resonances are dynamically generated in meson-baryon scattering, while the conventional quark model approach describes the baryon resonances as three-quark states with an excitation of one of the quarks.

The chiral unitary model is based on chiral perturbation theory (ChPT).^{7),8)} Imposing the unitarity condition, we can apply the ChPT in regions of higher energy than in the original perturbative calculation, and we can study properties of resonances generated by non-perturbative resummations. In the implementation of the unitarity condition, regularization of loop integrals brings parameters into this model, such as the three-momentum cut-off and the “subtraction constants” in the dimensional regularization.

In Refs. 1) and 5), s -wave scattering in meson and baryon systems with strangeness $S = -1$ was investigated by solving the Lippman-Schwinger equation in coupled channels, where the $\Lambda(1405)$ resonance is dynamically generated by meson-baryon scattering. In the regularization procedure, a form factor associated with the extended structure of hadrons is introduced in the kernel potential obtained by ChPT,¹⁾ while the loop integral is cut off in the three-momentum.⁵⁾ In Refs. 9), 10), 11), they

^{*}) Present address: ECT*, European Centre for Theoretical Studies in Nuclear Physics and Related Areas Villa Tambosi, Strada delle Tabarelle 286, I-38050 Villazzano (Trento), Italy.

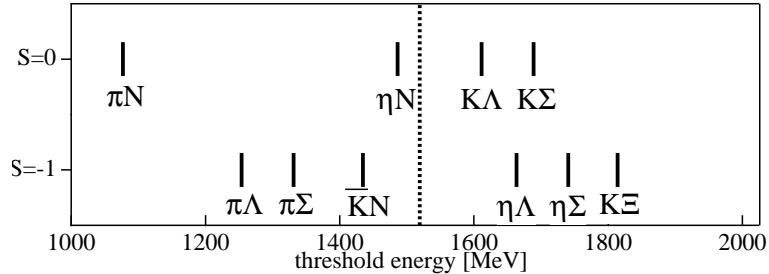


Fig. 1. Threshold energies of meson-baryon scattering in the $S = -1$ and $S = 0$ channels. The dotted line in the middle represents the averaged energy of all the meson-baryon thresholds.

extended the chiral unitary approach to other strangeness channels and obtained the baryonic resonances $\Lambda(1405)$, $N(1535)$, $\Lambda(1670)$, $\Sigma(1620)$ and $\Xi(1620)$ as dynamically generated objects. They used the dimensional regularization scheme with channel-dependent subtraction constants, a_i . In particular, the subtraction constants in $S = 0$ depended significantly on the channel, while, as reported in Ref. 12), it was found that a common subtraction constant in the $S = -1$ channel reproduces the total cross sections of the K^-p scattering as well as the $\Lambda(1405)$ properties. Note also that in a similar model with a different regularization scheme,¹³⁾ the position of the poles and their properties are changed.

In this work, we raise the question of whether or not such a channel dependence of subtraction constants could be dictated by the flavor $SU(3)$ breaking effects of an underlying theory. As we will discuss in detail, it is shown that the subtraction constants should not depend on the scattering channel in the $SU(3)$ limit.^{14),15)} The $SU(3)$ breaking should have a significant effect on the observed quantities. This is expected from, for instance, the large dependence of the threshold energies on the meson-baryon channels, as shown in Fig. 1. This is particularly true for $S = 0$, in which case the lowest threshold energy of the πN channel deviates considerably from the mean value. Furthermore, it was discussed in Ref. 16) that the number of channel-dependent subtraction constants for all $SU(3)$ channels exceeds the number of available counter terms of chiral order p^3 .

In order to study the above questions, we consider the following two cases:

- We use a common subtraction constant for all scattering channels and determine whether this simplified calculation works.
- When this method does not work, we introduce the flavor $SU(3)$ breaking effects into the interaction kernel.

In this way, we expect that the parameters in previous treatments could be controlled based on appropriate physical considerations. This would allow us to extend this method to other channels with predictive power. Note that the use of a single subtraction constant was first examined in Ref. 17). In this work, we concentrate on s wave scattering, because the p wave contribution to the total cross sections was shown to be small in the $S = -1$ channel in Ref. 18).

This paper contains a detailed study of the results in Ref. 15). In § 2, we present the formulation of the chiral unitary model. The calculation with a common

subtraction constant and comparison with the results of previous works are given in § 3. We then introduce the flavor $SU(3)$ breaking effects in the interaction kernel and present numerical results in § 4. We discuss the results and summarize this work in § 5.

§2. Formulation

In this section we briefly review the formulation of the chiral unitary model. We derive the basic interaction of meson-baryon scattering from the lowest-order chiral Lagrangian, and we maintain the unitarity of the S-matrix. There are several methods that recover the unitarity of the S-matrix such as solving the Bethe-Salpeter equation (BSE),⁵⁾ the inverse amplitude method (IAM),¹⁹⁾ the N/D method,¹²⁾ and so on. In this work, we adopt the N/D method,²⁰⁾ because this method provides a general form of the T-matrix using the dispersion relation and the analyticity of the inverse of the T-matrix. Recently, the N/D method has been applied to coupled channel meson-baryon scattering.^{21),12)} It was found that the final form of the T-matrix derived from the N/D method is essentially equivalent to the result given in Ref. 5) derived from the BSE.

The chiral Lagrangian for baryons in the lowest-order of the chiral expansion is given by²²⁾

$$\mathcal{L}_{\text{lowest}} = \text{Tr} \left(\bar{B} (i\mathcal{D} - M_0) B - D (\bar{B} \gamma^\mu \gamma_5 \{A_\mu, B\}) - F (\bar{B} \gamma^\mu \gamma_5 [A_\mu, B]) \right). \quad (2.1)$$

Here D and F are coupling constants. In Eq. (2.1), the covariant derivative \mathcal{D}_μ , the vector current V_μ , the axial vector current A_μ and the chiral field ξ are defined by

$$\mathcal{D}_\mu B = \partial_\mu B + i[V_\mu, B], \quad (2.2)$$

$$V_\mu = -\frac{i}{2}(\xi^\dagger \partial_\mu \xi + \xi \partial_\mu \xi^\dagger), \quad (2.3)$$

$$A_\mu = -\frac{i}{2}(\xi^\dagger \partial_\mu \xi - \xi \partial_\mu \xi^\dagger), \quad (2.4)$$

$$\xi(\Phi) = \exp\{i\Phi/\sqrt{2}f\}, \quad (2.5)$$

where f is the meson decay constant; here we take an averaged value $f = 1.15f_\pi$ with $f_\pi = 93$ MeV. The meson and baryon fields are expressed in $SU(3)$ matrix form as

$$B = \begin{pmatrix} \frac{1}{\sqrt{2}}\Sigma^0 + \frac{1}{\sqrt{6}}\Lambda & \Sigma^+ & p \\ \Sigma^- & -\frac{1}{\sqrt{2}}\Sigma^0 + \frac{1}{\sqrt{6}}\Lambda & n \\ \Xi^- & \Xi^0 & -\frac{2}{\sqrt{6}}\Lambda \end{pmatrix}, \quad (2.6)$$

$$\Phi = \begin{pmatrix} \frac{1}{\sqrt{2}}\pi^0 + \frac{1}{\sqrt{6}}\eta & \pi^+ & K^+ \\ \pi^- & -\frac{1}{\sqrt{2}}\pi^0 + \frac{1}{\sqrt{6}}\eta & K^0 \\ K^- & \bar{K}^0 & -\frac{2}{\sqrt{6}}\eta \end{pmatrix}. \quad (2.7)$$

In the Lagrangian (2.1), M_0 denotes the common mass of the octet baryons. However, we use the observed values of the baryon masses in the following calculations.

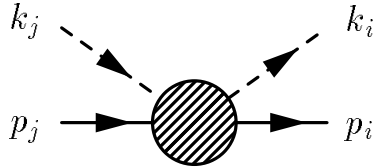


Fig. 2. Definition of the momentum variables. The dashed and solid lines represent mesons and baryons, respectively.

The mass splitting among the octet baryons in the Lagrangian level are introduced consistently with the $SU(3)$ breaking in § 4.

The s wave interactions at tree level come from the Weinberg-Tomozawa (WT) interaction, which is in the vector coupling term in the covariant derivative:

$$\mathcal{L}_{WT} = \text{Tr} \left(\bar{B} i \gamma^\mu \frac{1}{4f^2} [(\Phi \partial_\mu \Phi - \partial_\mu \Phi \Phi), B] \right). \quad (2.8)$$

From this Lagrangian, the meson-baryon scattering amplitude at tree level is given by

$$\begin{aligned} V_{ij}^{(WT)} &= -\frac{C_{ij}}{4f^2} \bar{u}(p_i)(\not{k}_i + \not{k}_j)u(p_j) \\ &= -\frac{C_{ij}}{4f^2} (2\sqrt{s} - M_i - M_j) \sqrt{\frac{E_i + M_i}{2M_i}} \sqrt{\frac{E_j + M_j}{2M_j}}, \end{aligned} \quad (2.9)$$

where the indices (i, j) denote the channels of the meson-baryon scattering, and M_i and E_i are the mass and the energy of the baryon in the channel i , respectively. These masses and factors come from the spinors of the baryons. It seems reasonable to use the common mass M_0 in the Lagrangian as in Ref. 12). However, in this paper we adopt the physical masses, as in Refs. 9), 10), 11). Indeed, we have checked that the results obtained with a common mass are qualitatively similar to the results obtained with observed masses. The channels (i, j) are shown in Table III of the Appendix. The kinematics of this vertex are depicted in Fig. 2, and s in Eq. (2.9) is defined as $s = (k + p)^2$. The last line is obtained in the center of mass frame with nonrelativistic reduction. The coefficient C_{ij} is fixed by chiral symmetry, and the explicit form of C_{ij} is given in Ref. 5) for $S = -1$ and in Ref. 10) for $S = 0$.

In the coupled channel formulation, the T-matrix takes a matrix form. The unitarity condition is guaranteed by the optical theorem, *i.e.* $-2\text{Im}[T_{ii}] = T_{ik}\rho_k T_{ki}^*$, which can be written as

$$2\text{Im}[T_{ii}^{-1}] = \rho_i, \quad (2.10)$$

where the normalization of the T-matrix is defined by

$$S_{ij} = 1 - i \left(\frac{\sqrt{2M_i} |\mathbf{q}_i| 2M_j |\mathbf{q}_j|}{4\pi\sqrt{s}} \right) T_{ij}.$$



Fig. 3. Diagrammatic interpretation of Eq. (2.18).

With the condition (2.10) and the dispersion relation for T_{ii}^{-1} , we find a general form of the T-matrix using the N/D method. Following Ref. 12), we write

$$T_{ij}^{-1}(\sqrt{s}) = \delta_{ij} \left(\tilde{a}_i(s_0) + \frac{s - s_0}{2\pi} \int_{s_i^+}^{\infty} ds' \frac{\rho_i(s')}{(s' - s)(s' - s_0)} \right) + \mathcal{T}_{ij}^{-1}, \quad (2.11)$$

where s_i^+ is the value of s at the threshold of the channel i , and s_0 is the subtraction point. The parameter $\tilde{a}_i(s_0)$ is the subtraction constant and is a free parameter within the N/D method. The matrix \mathcal{T}_{ij} is determined by the chiral perturbation theory, as discussed below. In the derivation of Eq. (2.11), we have ignored the left-hand cuts, which correspond to u -channel diagrams of the crossing symmetry.

Let us assume that the intermediate states of the meson-baryon scattering are composed of one octet meson and one octet baryon. We do not consider the case of multiple mesons and excited baryons, such as $\pi\pi N$ and $\pi\Delta$. In this case, the phase space ρ_i in Eq. (2.10) is written

$$\rho_i(\sqrt{s}) = \frac{2M_i |\mathbf{q}_i|}{4\pi\sqrt{s}}, \quad (2.12)$$

where \mathbf{q}_i is a three-momentum of the intermediate meson on the mass shell. Let us define the G function by

$$G_i(\sqrt{s}) = -\tilde{a}_i(s_0) - \frac{s - s_0}{2\pi} \int_{s_i^+}^{\infty} ds' \frac{\rho_i(s')}{(s' - s)(s' - s_0)}, \quad (2.13)$$

which takes the same form as, up to a constant, the ordinary meson-baryon loop function:

$$G_i(\sqrt{s}) = i \int \frac{d^4 q}{(2\pi)^4} \frac{2M_i}{(P - q)^2 - M_i^2 + i\epsilon} \frac{1}{q^2 - m_i^2 + i\epsilon}. \quad (2.14)$$

This integral should be regularized with an appropriate regularization scheme. In the dimensional regularization, the integral is calculated as

$$\begin{aligned} G_i(\sqrt{s}) = & \frac{2M_i}{(4\pi)^2} \left\{ a_i(\mu) + \ln \frac{M_i^2}{\mu^2} + \frac{m_i^2 - M_i^2 + s}{2s} \ln \frac{m_i^2}{M_i^2} \right. \\ & + \frac{\bar{q}_i}{\sqrt{s}} \left[\ln(s - (M_i^2 - m_i^2) + 2\sqrt{s}\bar{q}_i) + \ln(s + (M_i^2 - m_i^2) + 2\sqrt{s}\bar{q}_i) \right. \\ & \left. \left. - \ln(-s + (M_i^2 - m_i^2) + 2\sqrt{s}\bar{q}_i) - \ln(-s - (M_i^2 - m_i^2) + 2\sqrt{s}\bar{q}_i) \right] \right\}, \end{aligned} \quad (2.15)$$

channel-dependent a_i ($S = -1$)						
channel	$\bar{K}N$	$\pi\Sigma$	$\pi\Lambda$	$\eta\Lambda$	$\eta\Sigma$	$K\Xi$
a_i	-1.84	-2.00	-1.83	-2.25	-2.38	-2.67

channel-dependent a_i ($S = 0$)				
channel	πN	ηN	$K\Lambda$	$K\Sigma$
a_i	0.711	-1.09	0.311	-4.09

Table I. Channel-dependent subtraction constants a_i used in Refs. 9) and 10) with the regularization scale $\mu = 630$ MeV. For the $S = 0$ channel, although the original values of a_i are obtained with $\mu = 1200$ MeV, here we give the values of a_i corresponding to $\mu = 630$ MeV obtained using the relation $a(\mu') = a(\mu) + 2 \ln(\mu'/\mu)$.

where μ is the regularization scale, a_i is the subtraction constant, and \bar{q}_i is defined by

$$\bar{q}_i(\sqrt{s}) = \frac{\sqrt{(s - (M_i - m_i)^2)(s - (M_i + m_i)^2)}}{2\sqrt{s}}. \quad (2.16)$$

In the tree approximation, only the \mathcal{T}_{ij} term survives in Eq. (2.11). This may be identified with the WT interaction $V^{(WT)}$ in Eq. (2.9). Therefore, the resulting T-matrix is written

$$T^{-1} = -G + (V^{(WT)})^{-1}, \quad (2.17)$$

$$T = V^{(WT)} + V^{(WT)}GT. \quad (2.18)$$

This is the algebraic equation for the T-matrix, which corresponds to the integral BSE. The diagrammatic interpretation of Eq. (2.18) is displayed in Fig. 3.

The subtraction constants $a_i(\mu)$ in Eq. (2.15), in principle, would be related to the counter terms in the higher-order Lagrangian in the chiral perturbation theory. In previous works,^{9),10)} the subtraction constants a_i were fitted using the data for $\bar{K}N(S = -1)$ and $\pi N(S = 0)$ scatterings. In Table I, we list the subtraction constants used in Refs. 9) and 10). In the table, in order to compare the channel dependence of the subtraction constants, we take the regularization scale at $\mu = 630$ MeV in the both channels. Changing the regularization scale, the subtraction constants are simply shifted by $a(\mu') = a(\mu) + 2 \ln(\mu'/\mu)$. From this table, we see that the values of a_i values for $S = 0$ differ significantly. In the rest of this paper we refer to these parameters as the “channel-dependent a_i ”.

§3. Calculation with a common subtraction constant

In this section, we present calculations in which a single subtraction constant a is commonly used in the meson-baryon loop function (2.15) in order to determine the role of the channel-dependent a_i in reproducing the observed cross sections and the resonance properties. A channel-independent regularization scheme was first used in Ref. 17).

Let us first show that in the $SU(3)$ limit, together with the constraint in the chiral unitary model, there is only one subtraction constant.^{14),15)} Under $SU(3)$

symmetry, the scattering amplitudes of one octet meson and one octet baryon are composed of $SU(3)$ irreducible representations. The amplitudes satisfy the following scattering equation in each representation:

$$T(D) = V(D) + V(D)G(D)T(D) . \quad (3.1)$$

Here, D represents an $SU(3)$ irreducible representation, $D = 1, 8, 8, 10, \bar{10}$ and 27 . Therefore, on one hand, the functions G , or equivalently the subtraction constants a_i , are represented by diagonal matrices in the $SU(3)$ basis. On the other hand, because G functions are given as loop integrals, as shown in (14) and (15), they are also diagonal in the particle basis $(\pi^- p, \eta A, \dots)$. These observations imply that the subtraction constants are components of a diagonal matrix both in $SU(3)$ and in particle bases, which are transformed uniquely with a unitary matrix of $SU(3)$ Clebsch-Gordan coefficients,

$$a(D) = \sum_k U_{Dk} a_k (U^\dagger)_{kD} . \quad (3.2)$$

This can happen when the subtraction constants are proportional to unity. Hence, the subtraction constants are not dependent on the channel in the $SU(3)$ limit.

Now, we discuss the case $S = -1$, in which the subtraction constants a_i do not depend strongly on the channel, as shown in Table I. Therefore, it is expected that a calculation with a common value a gives a good description if we choose a suitable value.

Next we study the $S = 0$ channel using a common subtraction constant. Here, we find that common value a cannot simultaneously reproduce the resonance properties and the S_{11} amplitude in the low energy region.

In order to concentrate on the role of the subtraction constants and to deduce the channel dependence, we make the following simplifications for the calculations of the $S = -1$ and $S = 0$ channels:

- We use an averaged value for the meson decay constants, $f = 1.15f_\pi = 106.95$ MeV, while in Ref. 10), physical values were taken as $f_\pi = 93$ MeV, $f_K = 1.22f_\pi$, $f_\eta = 1.3f_\pi$.
- We do not include the effect of vector meson exchanges and $\pi\pi N$ channels to reproduce the $\Delta(1620)$ resonance, which were considered in Ref. 10).

With these simplifications, the calculations in the $S = -1$ and $S = 0$ channels are based on exactly the same formulation; the differences are in the flavor $SU(3)$ coefficients C_{ij} in Eq. (2.9) and in the channel-dependent subtraction constants.

3.1. The $S = -1$ channel ($\bar{K}N$ scattering)

In the $S = -1$ channel, the subtraction constants a_i obtained in Ref. 9) do not depend strongly on the channel, as shown in Table I. In Ref. 12), a common value of $a \sim -2$ was used. This value was “naturally” obtained from matching with the three-momentum cut-off regularization with $\Lambda = 630$ MeV. In both works, the total cross sections of the $K^- p$ scattering and the mass distribution of the $\pi\Sigma$ channel with $I = 0$, where the $\Lambda(1405)$ resonance is seen, were reproduced very well. In Ref. 9), the $\Lambda(1670)$ resonance was also obtained with the channel-dependent subtraction

constants, and its properties were investigated by analyzing the speed plots in the $I = 0$ channels.

Here we search for one common value a to be used in all channels for $S = -1$. In order to fix this common value a , we use threshold properties of the $\bar{K}N$ scattering, which are well observed in the branching ratios:^{23),24)}

$$\begin{aligned}\gamma &= \frac{\Gamma(K^- p \rightarrow \pi^+ \Sigma^-)}{\Gamma(K^- p \rightarrow \pi^- \Sigma^+)} \sim 2.36 \pm 0.04, \\ R_c &= \frac{\Gamma(K^- p \rightarrow \text{charged particles})}{\Gamma(K^- p \rightarrow \text{all})} \sim 0.664 \pm 0.011, \\ R_n &= \frac{\Gamma(K^- p \rightarrow \pi^0 \Lambda)}{\Gamma(K^- p \rightarrow \text{neutral particles})} \sim 0.189 \pm 0.015.\end{aligned}\quad (3.3)$$

After fitting, we find the optimal value $a = -1.96$, with which the threshold branching ratios are obtained, as shown in Table II. The result obtained using the common value $a = -1.96$ does not differ much from that obtained with channel-dependent values, and also the value $a = -1.96$ is close to the averaged value of the channel-dependent subtraction constants a_i , namely ~ -2.15 . Therefore, the threshold properties are not sensitive to such a fine tuning of the subtraction constants.

Using the common value $a = -1.96$, we calculate the total cross sections of the $K^- p$ scattering (Fig. 4, solid curves), the T-matrix amplitude of the $\bar{K}N$ scattering with $I = 0$ (Fig. 5, solid curves), and the mass distributions of the $\pi\Sigma$ channel with $I = 0$ (Fig. 6, solid curves). We also plot the results obtained with the channel-dependent a_i from the calculation given in Ref. 9) in Figs. 4, 5 and 6 as the dotted curves. Here, we find that the present calculations give results that are slightly different from those of the calculations with the channel-dependent a_i in the total cross sections and the $\pi\Sigma$ mass distributions. Therefore, the $\Lambda(1405)$ resonance is well reproduced with the common value $a = -1.96$, which is consistent with the results in Ref. 12). However, the resonance $\Lambda(1670)$ disappears when this common value a is used, as we see in the T-matrix amplitude of $\bar{K}N \rightarrow \bar{K}N$ with $I = 0$ in Fig. 5. As pointed out in Ref. 9), the $\Lambda(1670)$ resonance structure is very sensitive to the value of $a_{K\Sigma}$. Indeed, we have checked that the $\Lambda(1670)$ resonance is reproduced when we choose $a_{K\Sigma} \sim -2.6$ with the other a_i unchanged, *i.e.*, at -1.96 . In a recent publication, it was shown that the poles of $\Lambda(1405)$ and $\Lambda(1670)$ are simultaneously reproduced by taking into account the approximate crossing symmetry without considering explicitly the channel dependence.¹³⁾ The inclusion of the crossing symmetry is, however, beyond the scope of the present discussion.

If we choose $a = -2.6$ for all subtraction constants, the threshold branching ratios are obtained as $\gamma = 2.41$, $R_c = 0.596$ and $R_n = 0.759$, and the agreement with the experimental data becomes poor, as shown in Figs. 4 and 5. In particular, the $K^- p \rightarrow \bar{K}^0 n$ cross section is underestimated, and also the resonance structure of $\Lambda(1405)$ disappears in the $\pi\Sigma$ mass distribution (Fig. 6). As we change all subtraction constants from $a = -1.96$ to $a = -2.6$ gradually, the position of the peak of $\Lambda(1405)$ moves to the lower energy side and finally disappears under the $\pi\Sigma$ threshold. Therefore, using the common value $a \sim -2$ is essential to reproduce the

	γ	R_c	R_n
experiment	2.36 ± 0.04	0.664 ± 0.011	0.189 ± 0.015
channel-dependent a_i	1.73	0.629	0.195
common value a	1.80	0.624	0.225
$SU(3)$ breaking	2.19	0.623	0.179

Table II. Threshold branching ratios calculated with channel-dependent a_i , common value $a = -1.96$, and $a = -1.59$ with the $SU(3)$ breaking interaction. The experimental values were taken from Refs. 23) and 24).

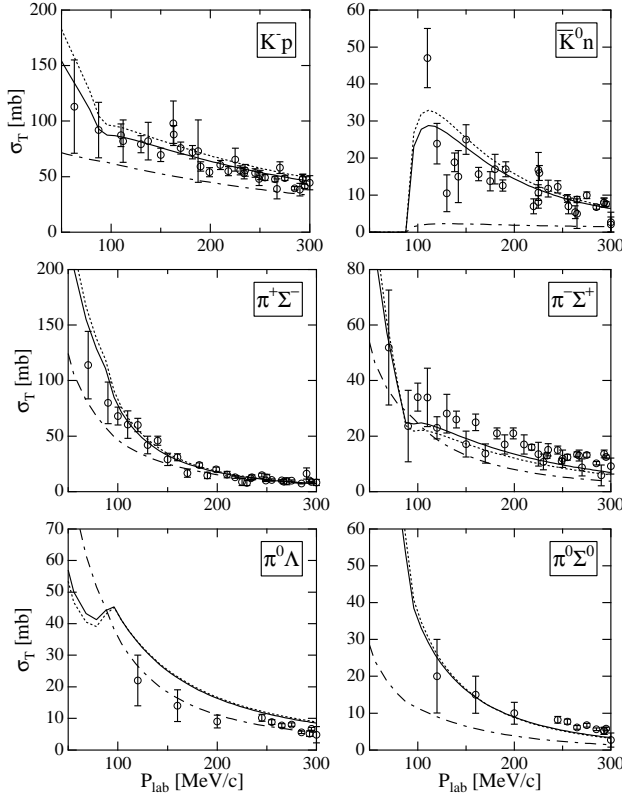


Fig. 4. Total cross sections of K^-p scattering ($S = -1$) as functions of P_{lab} , the three-momentum of the initial K^- in the laboratory frame. The dotted curve represent the results obtained with the channel-dependent a_i , the solid curves represent the results obtained with the common value $a = -1.96$, and the dash-dotted curves represent the results obtained with the common value $a = -2.6$. The open circles with error bars are experimental data taken from Refs. 25), 26), 27), 28), 29), 30), 31), 32), 33), 34), 35), 36).

resonance properties of $\Lambda(1405)$ and the total cross sections of the K^-p scattering in the low energy region.

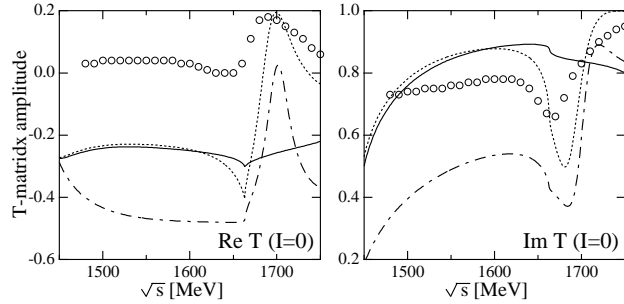


Fig. 5. Real and imaginary parts of the T-matrix amplitude of $\bar{K}N \rightarrow \bar{K}N$ with $I = 0$. The dotted curves represent the results obtained with the channel-dependent a_i , the solid curves represent the results obtained with the common value $a = -1.96$, and the dash-dotted curves represent the results obtained with the common value $a = -2.6$. The open circles are experimental data taken from Ref. 37).

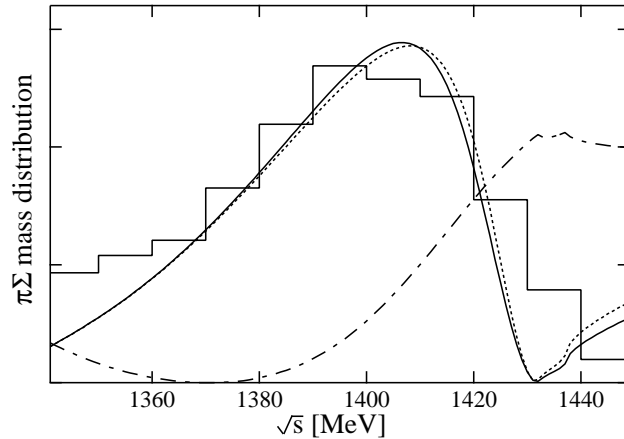


Fig. 6. The mass distributions of the $\pi\Sigma$ channel with $I = 0$. The dotted curve represents the result obtained with the channel-dependent a_i , the solid curve represents the result obtained with the common value $a = -1.96$, and the dash-dotted curve represents the result obtained with the common value $a = -2.6$. The histogram represents experimental data taken from Ref. 38).

3.2. The $S = 0$ channel (πN scattering)

In Ref. 10), the total cross sections of the $\pi^- p$ inelastic scattering and the resonance properties of the $N(1535)$ were reproduced well by using channel-dependent a_i . After the simplification applied to f and inelastic channels, the agreement with the data is still acceptable, as shown in Figs. 7 and 8 by the dotted curves, as long as channel-dependent a_i are employed. In the T-matrix elements of the πN scattering in the S_{11} channel, we see a kink structure around the energy $\sqrt{s} \sim 1500$ MeV, which corresponds to the $N(1535)$ resonance.¹⁰⁾

In the previous subsection, we obtained the common subtraction constant $a = -1.96$ with which the $\bar{K}N$ total cross sections and the $\Lambda(1405)$ properties are repro-

duced well. First, we use this common value of a for the $S = 0$ channel. It is worth noting that in Ref. 13), $N(1535)$ and $\Lambda(1405)$ were reproduced with the channel-independent renormalization scheme. Shown in Figs. 7 and 8 by the dash-dotted curves are the results with $a = -1.96$ for the total cross sections of the $\pi^- p \rightarrow \pi^0 \eta$, $K^0 \Lambda$ and $K^0 \Sigma$ scatterings, and the S_{11} T-matrix amplitude of $\pi N \rightarrow \pi N$. As can be seen in Figs. 7 and 8, the results with $a = -1.96$ in the $S = 0$ channel are far from the experimental data. In particular, in the $\pi^- p \rightarrow \eta n$ cross section, the threshold behavior disagrees with the experiment, and a resonance structure of $N(1535)$ disappears. In addition, as shown in Fig. 8, the T-matrix amplitude of the S_{11} channel is overestimated, and an unexpected resonance has been generated near $\sqrt{s} \sim 1250$ MeV.

Next, we search a single optimal subtraction constant within the $S = 0$ channel, because an unnecessary resonance is obtained with $a = -1.96$ at low energy. In order to avoid the appearance of such an unphysical resonance, we determine the common subtraction constant a so as to reproduce the observed data up to $\sqrt{s} = 1400$ MeV. The optimal value is found to be $a = 0.53$. The calculated S_{11} amplitude as well as the total cross sections are plotted in Figs. 7 and 8 by the solid curves. With this subtraction constant, the low energy behavior of the S_{11} amplitude of the πN scattering ($\sqrt{s} < 1400$ MeV) is well reproduced. Therefore, the scattering length is also reproduced. However, the $N(1535)$ resonance structure is not still generated. We have also checked that there is no pole in the scattering amplitudes in the second Riemann sheet. Therefore, we conclude that in the $S = 0$ channel we cannot reproduce simultaneously the $N(1535)$ resonance and the S_{11} amplitude at low energy if a single subtraction constant is used within the present approach.

§4. Flavor $SU(3)$ breaking interactions

In previous studies, it has been found that the channel-dependent subtraction constants a_i are crucial in order to reproduce important features of experimental data. In this section, we consider $SU(3)$ breaking terms of the chiral Lagrangian in order to see if the channel dependence in the subtraction constants can be absorbed into those terms. In this way, we are hoping that the number of free parameters can be reduced and that the origin of the channel dependence can be clarified.

4.1. Flavor $SU(3)$ breaking terms in the chiral Lagrangian

Here we introduce the flavor $SU(3)$ breaking effects in the chiral Lagrangian by the quark masses. They are obtained by assuming that the current quark mass matrix \mathbf{m} is transformed under the chiral transformation as $\mathbf{m} \rightarrow R\mathbf{m}L^\dagger$ and $\mathbf{m}^\dagger = \mathbf{m}$. Here we maintain isospin symmetry, that is, $\mathbf{m} = \text{diag}(\hat{m}, \hat{m}, m_s)$. Then, the $SU(3)$ breaking terms are given uniquely up to order $\mathcal{O}(m_q)$ as²²⁾

$$\begin{aligned} \mathcal{L}_{SB} = & -\frac{Z_0}{2} \text{Tr} \left(d_m \bar{B} \{ \xi \mathbf{m} \xi + \xi^\dagger \mathbf{m} \xi^\dagger, B \} + f_m \bar{B} [\xi \mathbf{m} \xi + \xi^\dagger \mathbf{m} \xi^\dagger, B] \right) \\ & - \frac{Z_1}{2} \text{Tr} (\bar{B} B) \text{Tr} (\mathbf{m} U + U^\dagger \mathbf{m}) , \end{aligned} \quad (4.1)$$

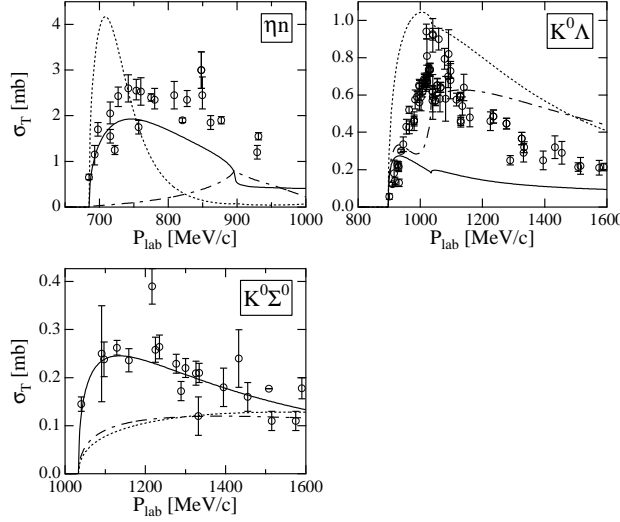


Fig. 7. Total cross sections of $\pi^- p$ scattering ($S = 0$) as functions of P_{lab} , the three-momentum of the initial π^- in the laboratory frame. The dotted curves represent the results obtained with channel-dependent a_i , the dash-dotted curves represent the results obtained with the common value $a = -1.96$, obtained for $S = -1$, and the solid curves represent the results obtained with the common value $a = 0.53$. The open circles with error bars are the experimental data taken from Refs. 39), 40), 41), 42), 43), 44), 45), 46), 47), 48), 49), 50), 51), 52), 53), 54), 55), 56), 57), 58).

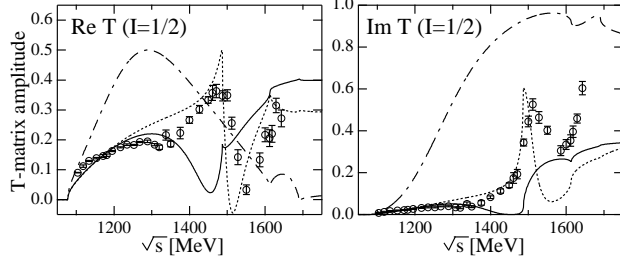


Fig. 8. Real and imaginary parts of the S_{11} T-matrix amplitudes of $\pi N \rightarrow \pi N$. The dotted curves represent the results obtained with channel-dependent a_i , the dash-dotted curves represent the results obtained with the common value $a = -1.96$, obtained for $S = -1$, and the solid curves show the results with the common value $a = 0.53$. The open circles with error bars are experimental data taken from Ref. 59).

where $f_m + d_m = 1$ and $U(\Phi) = \xi^2 = \exp\{i\sqrt{2}\Phi/f\}$. In this Lagrangian, there are three free parameters, $Z_0, Z_1, f_m/d_m$, which are determined by the baryon masses and the pion-nucleon sigma term, as we see below. For the quark mass, we take $m_s/\hat{m} = 26$, which is determined in ChPT from the meson masses. According to the chiral counting rule, these quark mass terms can be regarded as quantities of $\mathcal{O}(p^2)$, if we assume the Gell-Mann–Oakes–Renner relation,⁶⁰⁾ which implies $m_q \propto m_\pi^2$. In this work, we take into account only the terms in Eq. (4.1), and we do not consider other terms of order $\mathcal{O}(p^2)$. We explain the reason in the next subsection.

Expanding the Lagrangian (4.1) in powers of the meson fields, the zeroth order

terms contribute to the baryon mass splitting, which automatically satisfy the Gell-Mann-Okubo (GMO) mass formula.^{61),62)} By using the mass differences among the octet baryons, we determine the parameters Z_0 and f_m/d_m . The πN sigma term, which we take here to be $\sigma_{\pi N} = 36.4$ MeV, is used to determine the parameter Z_1 . The resulting parameters are given as

$$Z_0 = 0.528, \quad Z_1 = 1.56, \quad f_m/d_m = -0.31 \quad (4.2)$$

and $M_0 = 759$ MeV in the Lagrangian (2.1).

The meson-baryon interaction Lagrangian with $SU(3)$ breaking is obtained by picking up the terms with two meson fields. We find

$$\begin{aligned} \mathcal{L}_{SB}^{(2)} = & \frac{Z_0}{4f^2} \text{Tr} \left(d_m \bar{B} \{ (2\Phi \mathbf{m}\Phi + \Phi^2 \mathbf{m} + \mathbf{m}\Phi^2), B \} + f_m \bar{B} [(2\Phi \mathbf{m}\Phi + \Phi^2 \mathbf{m} + \mathbf{m}\Phi^2), B] \right) \\ & + \frac{Z_1}{f^2} \text{Tr}(\bar{B}B) \text{Tr}(\mathbf{m}\Phi^2). \end{aligned} \quad (4.3)$$

From this Lagrangian, the basic interaction is given by

$$\begin{aligned} V_{ij}^{(SB)} = & -\frac{1}{f^2} \left[Z_0 \left((A_{ij}^d d_m + A_{ij}^f f_m) \hat{m} + (B_{ij}^d d_m + B_{ij}^f f_m) m_s \right) \right. \\ & \left. + Z_1 \delta_{ij} D_i^{Z_1} \right] \sqrt{\frac{E_i + M_i}{2M_i}} \sqrt{\frac{E_j + M_j}{2M_j}}. \end{aligned} \quad (4.4)$$

The explicit forms of the coefficients A_{ij} , B_{ij} and D_i are given in the Appendix. These interaction terms are independent of the meson momenta, unlike the WT interaction (2.9).

Adding Eq. (4.4) to Eq. (2.9) and substituting them into Eq. (2.18), we obtain the unitarized T-matrix with the flavor $SU(3)$ breaking effects as

$$T = \left[1 - \left(V^{(WT)} + V^{(SB)} \right) G \right]^{-1} \left(V^{(WT)} + V^{(SB)} \right). \quad (4.5)$$

Because we have already fitted all parameters in the chiral Lagrangian, our parameters in the chiral unitary model with $SU(3)$ breaking effects are only the subtraction constants.

In the chiral Lagrangian, there are other $\mathcal{O}(p^2)$ terms symmetric in the $SU(3)$ flavor in addition to the above breaking terms, if we strictly follow the ordinary chiral counting rule in powers of the pseudoscalar meson momentum p and the quark mass m , where the GMOR relation fixes the ratio of m and p^2 . Indeed, it is known in chiral perturbation theory that at $\mathcal{O}(p^2)$ the πN scattering length is correctly obtained through a large cancellation between the $SU(3)$ breaking term and a symmetric term,^{63),64)} because the lowest-order, *i.e.* the Weinberg-Tomozawa term, already provides a sufficiently good result. This would imply that only the inclusion of the breaking term would be inconsistent with the cancellation.

However, in the present work, the symmetric terms are not taken into account for the following reasons. 1) These terms are not responsible for the symmetry

breaking which we would like to study in this paper. 2) The purpose of the present work is to investigate baryon resonances as dynamically generated objects. The symmetric terms of order $\mathcal{O}(p^2)$ may contain information regarding resonances,⁶⁵⁾ as shown for the role of the ρ meson in $\pi\pi$ scattering.⁶⁶⁾ The inclusion of some of the symmetric terms would introduce intrinsic properties of genuine resonances that originate from the quarks. 3) In our calculation, the πN scattering length is qualitatively reproduced well without the $\mathcal{O}(p^2)$ symmetric terms, because the subtraction constants in the chiral unitary approach are adjustable parameters determined by the threshold branching ratio Eq. (3.3). Strictly speaking, as argued in Ref. 12), the subtraction constants appear as $\mathcal{O}(p^3)$ quantities in the chiral expansion of the amplitude obtained in the unitary approach, because they originate from the loop integral. Therefore, they should not cancel the quark mass terms, which are counted as $\mathcal{O}(p^2)$. Nevertheless, we have room to interpret the subtraction constants as containing some of the $\mathcal{O}(p^2)$ terms that we do not take into account explicitly, as the parameter fitting is carried out for the full amplitudes obtained in the unitarity resummation at the physical threshold, and, as we see below, the threshold ratios are qualitatively reproduced much better than ChPT at lowest-order. This implies that some partial contributions of the symmetric terms are taken into account as constant values at the threshold.

In order to demonstrate the third point above, let us introduce another set of parameters a'_i that originate in the \mathcal{T}_{ij}^{-1} term in Eq. (2.11),

$$T_{ij}^{-1}(\sqrt{s}) = \delta_{ij} \left(\tilde{a}_i(s_0) + \frac{s - s_0}{2\pi} \int_{s_i^+}^{\infty} ds' \frac{\rho_i(s')}{(s' - s)(s' - s_0)} \right) + a'_i \delta_{ij} + \mathcal{T}_{ij}^{-1} . \quad (4.6)$$

Here, we assume that the parameters a'_i form a diagonal matrix in the channel space. Note that the parameters a'_i are introduced as quantities that are not related to the regularization of the loop integral, but they should be determined by ChPT. Now the parameters a'_i can be related to the coefficients of the $\mathcal{O}(p^2)$ symmetric Lagrangian. They are expressed as combinations of the two meson momenta

$$p_1^2, \quad p_2^2, \quad p_1 \cdot p_2, \quad \sigma_{\mu\nu} p_1^\mu p_2^\nu , \quad (4.7)$$

with subscripts 1 and 2 indicating the initial and final states, respectively. The last term does not contribute to the s -wave amplitude, and due to the symmetry under interchanges of 1 and 2 mesons, the coefficients of p_1^2 and p_2^2 should be the same. Therefore we have two independent coefficients. It is appropriate to consider the complete set of p^2 terms in the interaction kernel in order to strictly maintain consistency with ChPT and to achieve better agreement with the amplitudes. Once again, however, here we would like to study the $SU(3)$ breaking effect on the excited baryons as dynamically generated objects. In our procedure, the $SU(3)$ breaking is considered in the chiral perturbation theory completely, but without properties of genuine resonances.

As seen in Eq. (4.6), the parameters a'_i can be absorbed into the subtraction constants \tilde{a}_i , as $\tilde{a}_i \rightarrow \tilde{a}_i + a'_i$. Furthermore, $SU(3)$ symmetry reduces \tilde{a}_i to a single parameter, \tilde{a} . Hence, by adjusting \tilde{a} , we can use one degree of freedom of a' to fit

the low energy data. The introduction of a' is equivalent to the replacement

$$G \rightarrow G + a' . \quad (4.8)$$

Now, we expand the unitarized amplitude (4.5) in terms of the small meson momentum p , assuming that a' is an $\mathcal{O}(p^0)$ quantity, as

$$\begin{aligned} T &= V^{(WT)} + V^{(SB)} + (V^{(WT)} + V^{(SB)})(G + a')(V^{(WT)} + V^{(SB)}) + \dots \\ &= \underbrace{V^{(WT)}}_{p^1} + \underbrace{V^{(SB)} + V^{(WT)}a'V^{(WT)}}_{p^2} + V^{(WT)}GV^{(WT)} + \dots . \end{aligned} \quad (4.9)$$

The third term in the second line, $V^{(WT)}a'V^{(WT)}$, can play the role of an interaction derived from the p^2 Lagrangian and may cancel the $V^{(SB)}$ contribution to the scattering length when we choose $\tilde{a} + a'$ such that the low energy amplitude is reproduced.

4.2. The $S = -1$ channel

We follow the same procedures here as in the calculations without the $SU(3)$ breaking terms. First, we determine the common subtraction constant a from the threshold branching ratios (3.3). The optimal value is found to be $a = -1.59$. With this value, the total cross sections of the K^-p scattering, the $\pi\Sigma$ mass distribution, and the scattering amplitude of $\bar{K}N \rightarrow \bar{K}N$ with $I = 0$ are plotted in Figs. 9, 10 and 11 by the dash-dotted curves. As seen in Fig. 9, for all the total cross sections, the inclusion of the $SU(3)$ breaking terms with the common value a causes the agreement with data to become worse, although the threshold branching ratios are produced much better than in the previous works, as seen in Table II.

In the $\pi\Sigma$ mass distribution shown in Fig. 11 (the dash-dotted curve), a sharp peak is seen, in obvious contradiction with the observed spectrum. This means that the important resonance structure of $\Lambda(1405)$ has been lost. However, we find two poles of the T-matrix amplitude at $z_1 = 1424 - 1.6i$ and $z_2 = 1389 - 135i$ in the second Riemann sheet. It is reported that there are two poles in the T-matrix amplitude around the energy region of $\Lambda(1405)$ in Refs. 67), 12), 68), 69), 70), 13). A detailed study of the two poles for $\Lambda(1405)$ has recently been done from the viewpoint of the $SU(3)$ flavor symmetry in Ref. 14), and it has also been argued in the case of reaction processes.^{71), 72)} The inclusion of the $SU(3)$ breaking terms does not change this conclusion, although the positions of the poles change.

We also calculate the total cross sections and the $\pi\Sigma$ mass distribution with the physical values of the meson decay constants, $f_\pi = 93$ MeV, $f_K = 1.22f_\pi$, $f_\eta = 1.3f_\pi$. The calculated results are represented in Figs. 9, 10 and 11 by the solid curves. The optimal value of the subtraction constants is $a = -1.68$, and with this value, the threshold branching ratios are reproduced as $\gamma = 2.35$, $R_c = 0.626$ and $R_n = 0.172$. The $SU(3)$ breaking effect on the meson decay constants is not so large in the total cross sections, as seen in the figures. However, the shape of the peak seen in the $\pi\Sigma$ mass distribution becomes wider than that in the calculation with the averaged meson decay constant.

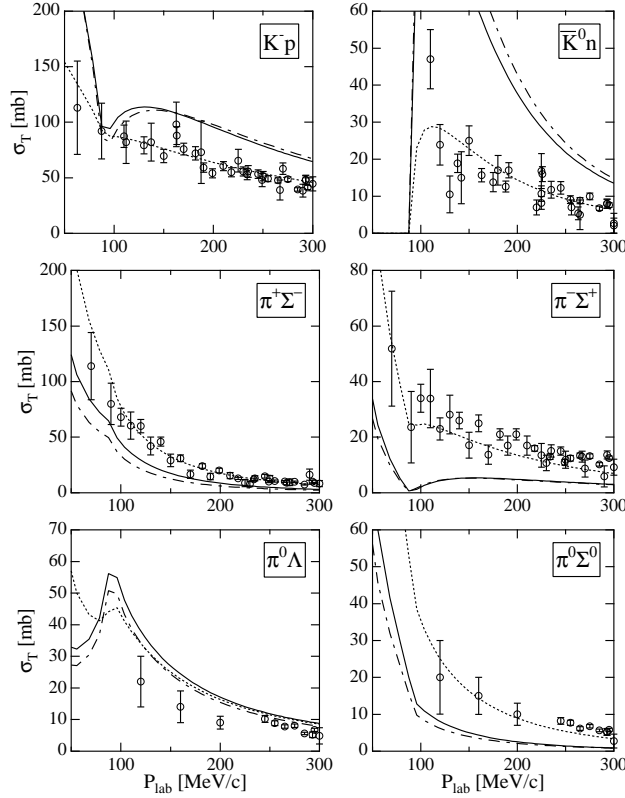


Fig. 9. Total cross sections of $K^- p$ scattering ($S = -1$) as functions of P_{lab} , the three-momentum of the initial K^- in the laboratory frame. The dotted curves represent the results obtained with the common value $a = -1.96$, the dash-dotted curves represent the results obtained including the $SU(3)$ breaking with the common value $a = -1.59$, and the solid curves represent the results obtained including the $SU(3)$ breaking and the physical f with the common value $a = -1.68$. The open circles with error bars are experimental data taken from Refs. 25), 26), 27), 28), 29), 30), 32), 33), 31), 34), 35), 36).

Indeed, we again find two poles in the scattering amplitudes at $z'_1 = 1424 - 2.6i$ and $z'_2 = 1363 - 87i$ in the second Riemann sheet. Compared with the poles z_1 and z_2 obtained in the above calculation, the position of the pole z'_2 moves to the lower energy side and approaches the real axis. The reason why the position of z'_2 changes can be understood as follows. Because z_2 has a large imaginary part, which implies a large width, and only the $\pi\Sigma$ channel is open in this energy region, the resonance represented by the pole z_2 has a strong coupling to the $\pi\Sigma$ channel. This fact implies that the position of the pole z_2 is sensitive to the $\pi\Sigma$ interaction. In the present calculation, the pion decay constant (93 MeV) is smaller than the averaged value (106.95 MeV) used in the above calculation, so that the attractive interaction of $\pi\Sigma$ becomes stronger. This shifts the position of the pole z_2 to the lower energy side. Simultaneously, this suppresses the phase space of the decay of the resonance to the $\pi\Sigma$ channel, and hence, the position of the pole approaches the real axis.

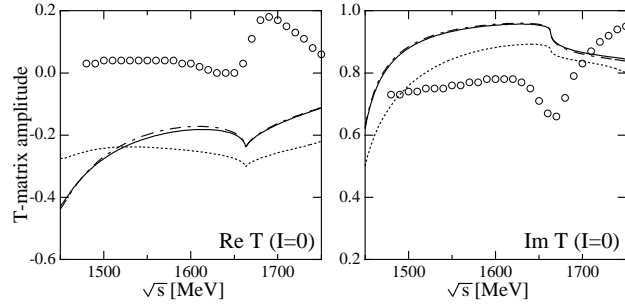


Fig. 10. Real and imaginary parts of the T-matrix amplitude of $\bar{K}N \rightarrow \bar{K}N$ with $I = 0$. The dotted curves represent the results obtained with the common value $a = -1.96$, the dash-dotted curves represent the results obtained including the $SU(3)$ breaking with the common value $a = -1.59$, and the solid curves represent the results obtained including the $SU(3)$ breaking and the physical f with the common value $a = -1.68$. The open circles are the experimental data taken from Ref. 37).

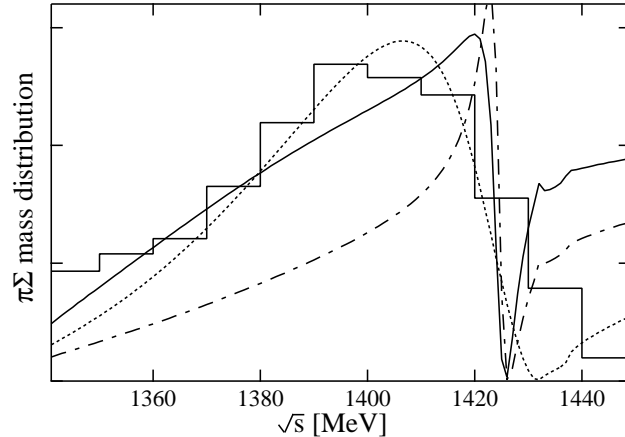


Fig. 11. Mass distributions of the $\pi\Sigma$ channel with $I = 0$. The dotted curve represents the result obtained with the common value $a = -1.96$, the dash-dotted curve represents the result obtained including the $SU(3)$ breaking with the common value $a = -1.59$, and the solid curve represents the result obtained including the $SU(3)$ breaking and the physical f with the common value $a = -1.68$. The histogram represents the experimental data taken from Ref. 38).

4.3. The $S = 0$ channel

Here we present calculations in the $S = 0$ channel with the $SU(3)$ breaking terms. With a common value $a \sim -1.5$, with which the threshold properties are reproduced well in the $S = -1$ channel, we still obtain a large contribution in the S_{11} πN scattering amplitude at low energy, as in the calculation without the $SU(3)$ breaking effects. From this analysis, it is found that the low energy behavior of the πN scattering cannot be reproduced as long as we use the common value $a \sim -2$, even if we introduce the $SU(3)$ breaking effects.

In order to search for the optimal value of the common subtraction constant within the $S = 0$ channel, we carried out a fitting of the T-matrix elements in the

πN S_{11} channel in the low energy region up to 1400 MeV. We find $a = 1.33$. The results including the $SU(3)$ breaking effects with $a = 1.33$ are represented as dash-dotted curves in Figs. 12 and 13. As seen in Fig. 13, the fitting is accurate up to $\sqrt{s} \sim 1400$ MeV, while, however, the resonance structure does not appear near energies of $N(1535)$.

Finally, we present the calculations with the physical values of the meson decay constants in Figs. 12 and 13 (solid curves). The optimal value of the common subtraction constant is found to be $a = 2.24$. The results with the physical meson decay constants and $a = 2.24$ are very similar to the results of the calculation with the averaged value of the decay constants and $a = 1.33$. In this sense, the $SU(3)$ breaking effect of the meson decay constant f is absorbed into the change of the common subtraction constant a .

In closing this section, we conclude that even if we introduce the $SU(3)$ breaking effects at the Lagrangian level, the $SU(3)$ breaking in the channel-dependent subtraction constants a_i cannot be absorbed into the $SU(3)$ breaking effects in the fundamental interactions in both the $S = -1$ and $S = 0$ channels.

§5. Summary and discussion

In this work, first we attempted to use a single common subtraction constant in order to describe meson-baryon scattering and baryon resonance in a unified way. In the $S = -1$ channel, $a \sim -2$ is fixed from the threshold branching ratios of the $K^- p$ scattering. With this parameter values, the total cross sections of the $K^- p$ scattering are reproduced well, as well as the mass distribution for $\Lambda(1405)$. However, in this case the $\Lambda(1670)$ resonance cannot be reproduced. The subtraction constant $a \sim -2$ corresponds to $\Lambda = 630$ MeV in the three-momentum cut-off regularization of the meson-baryon loop integral.¹²⁾ This value is consistent with that often used in single nucleon processes.⁷³⁾ The elementary interaction of the $\bar{K}N$ system is sufficiently attractive, and a resummation of the coupled channel interactions causes the $\Lambda(1405)$ resonance to appear at the correct position, by imposing the unitarity condition and by using the natural value for the cut-off parameter. Hence, the wave function of $\Lambda(1405)$ is largely dominated by the $\bar{K}N$ component.

On the other hand, in the $S = 0$ channel, if one uses the natural value for the subtraction constant, as in the $S = -1$ channel, the attraction of the meson-baryon interaction becomes so strong that an unexpected resonance is generated near $\sqrt{s} \sim 1250$ MeV. Therefore, a repulsive component is necessary to reproduce the observed πN scattering. The fitted subtraction constant using the low energy πN scattering amplitude is $a \sim 0.5$. With this value, however, the $N(1535)$ resonance is not generated, while the agreement among the cross sections of $\pi^- p \rightarrow \eta n$ is rather good, due to the threshold effects.

The unitarized amplitudes are very sensitive to the attractive component of the interaction. The interaction terms of the ChPT alone do not explain all scattering amplitudes simultaneously. Rather, they must be complemented by subtraction constants in the chiral unitary model. For small a , the interaction becomes more attractive, and for large a , less attractive. For $S = 0$, we need to choose $a \sim 0.5$ in

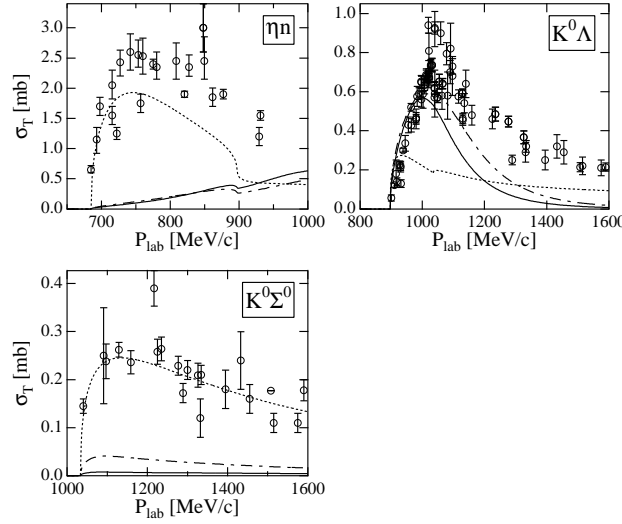


Fig. 12. Total cross sections of π^-p scattering ($S = 0$) as functions of P_{lab} , the three-momentum of the initial π^- in the laboratory frame. The dotted curve represent the results obtained with the common value $a = 0.53$, the dash-dotted curves represent the results obtained including the $SU(3)$ breaking interaction with the common value $a = 1.33$, and the solid curves represent the results obtained including the $SU(3)$ breaking and the physical f with the common value $a = 2.24$. The open circles with error bars are experimental data taken from Refs. 39), 40), 41), 42), 43), 44), 45), 46), 47), 48), 49), 50), 51), 52), 53), 54), 55), 56), 57), 58).

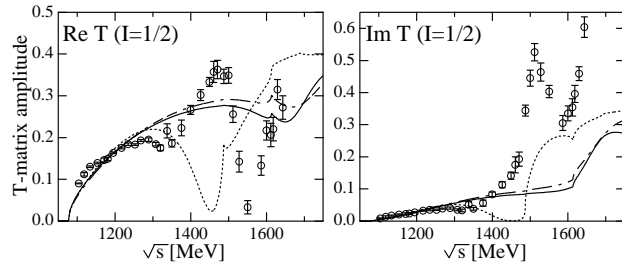


Fig. 13. Real and imaginary parts of the S_{11} T-matrix amplitudes of $\pi N \rightarrow \pi N$. The dotted curves represent the results obtained with the common value $a = 0.53$, the dash-dotted curves represent the results obtained including the $SU(3)$ breaking interaction with the common value $a = 1.33$, and the solid curves represent the results obtained including the $SU(3)$ breaking and the physical f with the common value $a = 2.24$. The open circles with error bars are experimental data taken from Ref. 59).

order to suppress the attraction from the πN interaction, in contrast to the situation for the natural value $a \sim -2$ in the $S = -1$ channel. Therefore, it is not possible to reproduce both the $\Lambda(1405)$ resonance properties and the low energy πN scattering with a common subtraction constant within the present framework.

Generally speaking, the chiral unitary approach is a powerful phenomenological method. It can reproduce cross sections and generate s wave resonances dynamically, once the subtraction constants are determined appropriately, using experimental

data. However, it is not straightforward to apply the method to channels for which there are not sufficient experimental data, because they are needed to determine the subtraction constants, unless we employ a channel-independent renormalization scheme, as in Refs. 17), 6) and 13).

Next, we introduced the flavor $SU(3)$ breaking Lagrangian, with the hope that the channel dependence in the subtraction constants would be absorbed into the coefficients in the chiral Lagrangian. These coefficients can be determined from other observables, and hence they are more controllable than the subtraction constants, which have to be fitted to the experimental data. However, the channel dependence of the subtraction constants in each strangeness channel cannot be replaced by the $SU(3)$ breaking Lagrangian, although we have exhausted possible breaking sources up to order $\mathcal{O}(m_q)$.

Therefore, in the present framework, in which the Weinberg-Tomozawa term and symmetry breaking terms are taken into account, a suitable choice of the channel-dependent subtraction constants is essential. Theoretically, it would be very important to obtain a microscopic explanation of the origin of the channel-dependent subtraction constants. One possibility is to consider quark degrees of freedom, which can generate genuine resonance states. Another possibility to solve this problem is to employ interaction terms up to order p^3 with the channel-independent renormalization scheme.⁶⁾ Further investigations should be carried out in order to better understand the nature of baryon resonances.

Acknowledgements

We would like to thank Profs. E. Oset, H. -Ch. Kim and W. Weise for useful discussions.

Appendix A — Coefficients of the $SU(3)$ Breaking Interaction —

Here, we derive the coefficients of the flavor $SU(3)$ breaking terms in the meson-baryon interactions. The corresponding Lagrangian is given by

$$\begin{aligned} \mathcal{L}_{SB}^{(2)} = & \frac{Z_0}{4f^2} \text{Tr} \left(d_m \bar{B} \{ (2\Phi \mathbf{m} \Phi + \Phi^2 \mathbf{m} + \mathbf{m} \Phi^2), B \} + f_m \bar{B} [(2\Phi \mathbf{m} \Phi + \Phi^2 \mathbf{m} + \mathbf{m} \Phi^2), B] \right) \\ & + \frac{Z_1}{f^2} \text{Tr}(\bar{B} B) \text{Tr}(\mathbf{m} \Phi^2). \end{aligned} \quad (\text{A.1})$$

From this Lagrangian, the basic interaction at tree level is given by

$$\begin{aligned} V_{ij}^{(SB)} = & -\frac{1}{f^2} \left[Z_0 \left((A_{ij}^d d_m + A_{ij}^f f_m) \hat{m} + (B_{ij}^d d_m + B_{ij}^f f_m) m_s \right) \right. \\ & \left. + Z_1 \delta_{ij} D_i^{Z_1} \right] \sqrt{\frac{E_i + M_i}{2M_i}} \sqrt{\frac{E_j + M_j}{2M_j}}, \end{aligned} \quad (\text{A.2})$$

where the coefficients A , B and D are the numbers in matrix form, and the indices (i, j) denote the channels of the meson-baryon scattering, as shown in Table III.

Table III. Channels of meson-baryon scattering. In this work, we carried out calculation for the channels in $(S = -1, Q = 0)$ and $(S = 0, Q = 0)$.

Y	S	I_3	Q	channels
-2	-3	1	0	$K^0\Xi^0$
		0	-1	$K^-\Xi^0, \bar{K}^0\Xi^-$
		-1	-2	$K^-\Xi^-$
-1	-2	$\frac{3}{2}$	1	$\pi^+\Xi^0, \bar{K}^0\Sigma^+$
		$\frac{1}{2}$	0	$\pi^0\Xi^0, \pi^+\Xi^-, \eta\Xi^0, \bar{K}^0\Lambda, \bar{K}^0\Sigma^0, K^-\Sigma^+$
		$-\frac{1}{2}$	-1	$\pi^0\Xi^-, \pi^-\Xi^0, \eta\Xi^-, K^-\Lambda, K^-\Sigma^0, \bar{K}^0\Sigma^-$
		$-\frac{3}{2}$	-2	$\pi^-\Xi^-, K^-\Sigma^-$
0	-1	2	2	$\pi^+\Sigma^+$
		1	1	$\bar{K}^0p, \pi^0\Sigma^+, \pi^+\Sigma^0, \pi^+\Lambda, \eta\Sigma^+, K^+\Xi^0$
		0	0	$K^-p, \bar{K}^0n, \pi^0\Lambda, \pi^0\Sigma^0, \eta\Lambda, \eta\Sigma^0, \pi^+\Sigma^-, \pi^-\Sigma^+, K^+\Xi^-, K^0\Xi^0$
		-1	-1	$K^-n, \pi^0\Sigma^-, \pi^-\Sigma^0, \pi^-\Lambda, \eta\Sigma^-, K^0\Xi^-$
		-2	-2	$\pi^-\Sigma^-$
1	0	$\frac{3}{2}$	2	$\pi^+p, K^+\Sigma^+$
		$\frac{1}{2}$	1	$\pi^0p, \pi^+n, \eta p, K^+\Lambda, K^+\Sigma^0, K^0\Sigma^+$
		$-\frac{1}{2}$	0	$\pi^0n, \pi^-p, \eta n, K^0\Lambda, K^0\Sigma^0, K^+\Sigma^-$
		$-\frac{3}{2}$	-1	$\pi^-n, K^0\Sigma^-$
2	1	1	2	K^+p
		0	1	K^+n, K^0p
		-1	0	K^0n

Table IV. Form of $D_i^{Z_1}$.

meson	π	K, \bar{K}	η
$D_i^{Z_1}$	$2\hat{m}$	$\hat{m} + m_s$	$\frac{2}{3}(\hat{m} + 2m_s)$

These channels are specified by two quantum numbers, the hypercharge, Y , and the third component of isospin I_3 , or equivalently the strangeness, S , and the electric charge, Q , through the Gell-Mann–Nakano–Nishijima relation^{74),75)}

$$Q = T_3 + \frac{Y}{2}, \quad S = Y - B, \quad (\text{A.3})$$

where the baryon number is $B = 1$ for the meson-baryon scattering.

The coefficient $D_i^{Z_1}$ is specified only by the meson in channel i , independently of the baryons, because $\text{Tr}(\bar{B}B)$ in the last term of Eq. (A.1) gives a common contribution to all baryons. Also, there is no off-diagonal component when the isospin symmetry is assumed. The explicit form of $D_i^{Z_1}$ is presented in Table IV. The values of the coefficients A and B are given in subsequent tables, as follows:

- Table VI ($S = 1, Q = 1$)
- Table VII ($S = -3, Q = -1$)
- Tables VIII and IX ($S = 0, Q = 0$)
- Tables X and XI ($S = -2, Q = -1$)
- Tables XII, XIII, XIV and XV ($S = -1, Q = 0$).

From these tables, the coefficients A and B for all the channels can be derived, using symmetry relations.

First, channels with equal S and unequal Q are related through the SU(2)

Table V. Quantum numbers for the channels i, j, i' and j'

channel	hypercharge			third component of isospin		
	meson	baryon	total	meson	baryon	total
i	y_i	$Y - y_i$	Y	i_{3i}	$I_3 - i_{3i}$	I_3
j	y_j	$Y - y_j$	Y	i_{3j}	$I_3 - i_{3j}$	I_3
i'	$-y_i$	$-Y + y_i$	$-Y$	$-i_{3i}$	$-I_3 + i_{3i}$	$-I_3$
j'	$-y_j$	$-Y + y_j$	$-Y$	$-i_{3j}$	$-I_3 + i_{3j}$	$-I_3$

Table VI. $A_{ij}^d, A_{ij}^f, B_{ij}^d$ and $B_{ij}^f (S = 1, Q = 1)$

	A_{ij}^d		A_{ij}^f		B_{ij}^d		B_{ij}^f	
	$K^+ n$	$K^0 p$	$K^+ n$	$K^0 p$	$K^+ n$	$K^0 p$	$K^+ n$	$K^0 p$
$K^+ n$	$\frac{1}{2}$	$\frac{1}{2}$	$-\frac{1}{2}$	$\frac{1}{2}$	$\frac{1}{2}$	$\frac{1}{2}$	$-\frac{1}{2}$	$\frac{1}{2}$
$K^0 p$		$\frac{1}{2}$		$-\frac{1}{2}$		$\frac{1}{2}$		$-\frac{1}{2}$

Table VII. $A_{ij}^d, A_{ij}^f, B_{ij}^d$ and $B_{ij}^f (S = -3, Q = -1)$

	A_{ij}^d		A_{ij}^f		B_{ij}^d		B_{ij}^f	
	$K^- \Xi^0$	$\bar{K}^0 \Xi^-$						
$K^0 \Xi^-$	$\frac{1}{2}$	$\frac{1}{2}$	$\frac{1}{2}$	$-\frac{1}{2}$	$\frac{1}{2}$	$\frac{1}{2}$	$\frac{1}{2}$	$-\frac{1}{2}$
$K^- \Xi^0$		$\frac{1}{2}$		$\frac{1}{2}$		$\frac{1}{2}$		$\frac{1}{2}$

Clebsch-Gordan coefficients due to the isospin symmetry. This is the relation among the channels in the block separated by the horizontal lines in Table III. Second, the coefficients of the sector (Y, I_3) are related with those of $(-Y, -I_3)$. Let us consider the channels (i, j) and (i', j') in the sectors (Y, I_3) and $(-Y, -I_3)$, respectively, as shown in Table V. Then, the coefficients of the sector $(-Y, -I_3)$ are given by

$$\begin{aligned} A_{i'j'}^d(-Y, -I_3) &= A_{ij}^d(Y, I_3), & A_{i'j'}^f(-Y, -I_3) &= -A_{ij}^f(Y, I_3), \\ B_{i'j'}^d(-Y, -I_3) &= B_{ij}^d(Y, I_3), & B_{i'j'}^f(-Y, -I_3) &= -B_{ij}^f(Y, I_3). \end{aligned} \quad (\text{A.4})$$

Comparing Table VI ($Y = 2, I_3 = 0$) and Table VII ($Y = -2, I_3 = 0$), we find that the relation (A.4) is satisfied. Also, using the relation (A.4), the coefficients of the sector $(S = -2, Q = 0)$ are obtained from the tables of the sector $(S = 0, Q = 0)$. For example, if we specify (i, j) to be $(\pi^0 n, K^0 \Lambda)$, the corresponding (i', j') is $(\pi^0 \Xi^0, \bar{K}^0 \Lambda)$. The coefficients for (i', j') are obtained as $A_{i'j'}^d = \sqrt{3}/8$, $A_{i'j'}^f = -3\sqrt{3}/8$, $B_{i'j'}^d = 1/(8\sqrt{3})$ and $B_{i'j'}^f = -\sqrt{3}/8$. In this way, we can derive all the coefficients that are not shown in the tables.

References

- 1) N. Kaiser, P. B. Siegel and W. Weise, Nucl. Phys. A **594** (1995), 325.
- 2) N. Kaiser, P. B. Siegel and W. Weise, Phys. Lett. B **362** (1995), 23.
- 3) N. Kaiser, T. Waas and W. Weise, Nucl. Phys. A **612** (1997), 297.
- 4) B. Krippa, Phys. Rev. C **58** (1998), 1333.
- 5) E. Oset and A. Ramos, Nucl. Phys. A **635** (1998), 99.
- 6) M. F. M. Lutz and E. E. Kolomeitsev, Nucl. Phys. A **700** (2002), 193.
- 7) S. Weinberg, Physica **A96**, 327 (1979).
- 8) J. Gasser and H. Leutwyler, Nucl. Phys. B **250** (1985), 465.
- 9) E. Oset, A. Ramos and C. Bennhold, Phys. Lett. B **527** (2002), 99.

Table VIII. A_{ij}^d and $A_{ij}^f(S = 0, Q = 0)$

	A_{ij}^d					A_{ij}^f						
	$\pi^0 n$	$\pi^- p$	ηn	$K^0 \Lambda$	$K^0 \Sigma^0$	$K^+ \Sigma^-$	$\pi^0 n$	$\pi^- p$	ηn	$K^0 \Lambda$	$K^0 \Sigma^0$	$K^+ \Sigma^-$
$\pi^0 n$	1	0	$-\frac{1}{\sqrt{3}}$	$\frac{\sqrt{3}}{8}$	$\frac{3}{8}$	$-\frac{3}{4\sqrt{2}}$	1	0	$-\frac{1}{\sqrt{3}}$	$\frac{3\sqrt{3}}{8}$	$-\frac{3}{8}$	$-\frac{3}{4\sqrt{2}}$
$\pi^- p$		1	$\sqrt{\frac{2}{3}}$	$-\frac{\sqrt{6}}{8}$	$\frac{3}{4\sqrt{2}}$	0		1	$\sqrt{\frac{2}{3}}$	$-\frac{3\sqrt{6}}{8}$	$-\frac{3}{4\sqrt{2}}$	0
ηn			$\frac{1}{3}$	$-\frac{1}{24}$	$-\frac{1}{8\sqrt{3}}$	$\frac{1}{4\sqrt{6}}$			$\frac{1}{3}$	$-\frac{1}{8}$	$\frac{1}{8\sqrt{3}}$	$-\frac{1}{4\sqrt{6}}$
$K^0 \Lambda$				$\frac{5}{6}$	$-\frac{1}{2\sqrt{3}}$	$\frac{1}{\sqrt{6}}$				0	0	0
$K^0 \Sigma^0$					$\frac{1}{2}$	0				0		$\frac{1}{\sqrt{2}}$
$K^+ \Sigma^-$						$\frac{1}{2}$						$-\frac{1}{2}$

 Table IX. B_{ij}^d and $B_{ij}^f(S = 0, Q = 0)$

	B_{ij}^d					B_{ij}^f						
	$\pi^0 n$	$\pi^- p$	ηn	$K^0 \Lambda$	$K^0 \Sigma^0$	$K^+ \Sigma^-$	$\pi^0 n$	$\pi^- p$	ηn	$K^0 \Lambda$	$K^0 \Sigma^0$	$K^+ \Sigma^-$
$\pi^0 n$	0	0	0	$\frac{1}{8\sqrt{3}}$	$\frac{1}{8}$	$-\frac{1}{4\sqrt{2}}$	0	0	0	$\frac{\sqrt{3}}{8}$	$-\frac{1}{8}$	$-\frac{1}{4\sqrt{2}}$
$\pi^- p$		0	0	$-\frac{1}{4\sqrt{6}}$	$\frac{1}{4\sqrt{2}}$	0		0	0	$-\frac{\sqrt{6}}{8}$	$-\frac{1}{4\sqrt{2}}$	0
ηn			$\frac{4}{3}$	$\frac{5}{24}$	$\frac{8\sqrt{3}}{3}$	$-\frac{5}{4\sqrt{6}}$			$-\frac{4}{3}$	$\frac{5}{8}$	$-\frac{5}{8\sqrt{3}}$	$\frac{5}{4\sqrt{6}}$
$K^0 \Lambda$				$\frac{5}{6}$	$-\frac{1}{2\sqrt{3}}$	$\frac{1}{\sqrt{6}}$				0	0	0
$K^0 \Sigma^0$					$\frac{1}{2}$	0				0		$\frac{1}{\sqrt{2}}$
$K^+ \Sigma^-$						$\frac{1}{2}$						$-\frac{1}{2}$

 Table X. A_{ij}^d and $A_{ij}^f(S = -2, Q = -1)$

	A_{ij}^d					A_{ij}^f						
	$\pi^0 \Xi^-$	$\pi^- \Xi^0$	$\eta \Xi^-$	$K^- \Lambda$	$K^- \Sigma^0$	$\bar{K}^0 \Sigma^-$	$\pi^0 \Xi^-$	$\pi^- \Xi^0$	$\eta \Xi^-$	$K^- \Lambda$	$K^- \Sigma^0$	$\bar{K}^0 \Sigma^-$
$\pi^0 \Xi^-$	1	0	$\frac{1}{\sqrt{3}}$	$-\frac{\sqrt{3}}{8}$	$\frac{3}{8}$	$-\frac{3}{4\sqrt{2}}$	-1	0	$-\frac{1}{\sqrt{3}}$	$\frac{3\sqrt{3}}{8}$	$\frac{3}{8}$	$-\frac{3}{4\sqrt{2}}$
$\pi^- \Xi^0$		1	$\sqrt{\frac{2}{3}}$	$-\frac{\sqrt{6}}{8}$	$-\frac{3}{4\sqrt{2}}$	0		-1	$-\sqrt{\frac{2}{3}}$	$\frac{3\sqrt{6}}{8}$	$-\frac{3}{4\sqrt{2}}$	0
$\eta \Xi^-$			$\frac{4}{3}$	$-\frac{1}{24}$	$\frac{1}{8\sqrt{3}}$	$\frac{1}{4\sqrt{6}}$			$-\frac{4}{3}$	$\frac{1}{8}$	$\frac{1}{8\sqrt{3}}$	$\frac{1}{4\sqrt{6}}$
$K^- \Lambda$				$\frac{5}{6}$	$-\frac{1}{2\sqrt{3}}$	$\frac{1}{\sqrt{6}}$				0	0	0
$K^- \Sigma^0$					$\frac{1}{2}$	0				0		$\frac{1}{\sqrt{2}}$
$\bar{K}^0 \Sigma^-$						$\frac{1}{2}$						$\frac{1}{2}$

 Table XI. B_{ij}^d and $B_{ij}^f(S = -2, Q = -1)$

	B_{ij}^d					B_{ij}^f						
	$\pi^0 \Xi^-$	$\pi^- \Xi^0$	$\eta \Xi^-$	$K^- \Lambda$	$K^- \Sigma^0$	$\bar{K}^0 \Sigma^-$	$\pi^0 \Xi^-$	$\pi^- \Xi^0$	$\eta \Xi^-$	$K^- \Lambda$	$K^- \Sigma^0$	$\bar{K}^0 \Sigma^-$
$\pi^0 \Xi^-$	0	0	0	$-\frac{1}{8\sqrt{3}}$	$\frac{1}{8}$	$-\frac{1}{4\sqrt{2}}$	0	0	0	$\frac{\sqrt{3}}{8}$	$\frac{1}{8}$	$-\frac{1}{4\sqrt{2}}$
$\pi^- \Xi^0$		0	0	$-\frac{1}{4\sqrt{6}}$	$-\frac{1}{4\sqrt{2}}$	0		0	0	$\frac{3}{4\sqrt{6}}$	$-\frac{1}{4\sqrt{2}}$	0
$\eta \Xi^-$			$\frac{4}{3}$	$\frac{5}{24}$	$-\frac{5}{8\sqrt{3}}$	$-\frac{5}{4\sqrt{6}}$			$\frac{4}{3}$	$-\frac{1}{8}$	$-\frac{5}{8\sqrt{3}}$	$-\frac{5}{4\sqrt{6}}$
$K^- \Lambda$				$\frac{5}{6}$	$-\frac{1}{2\sqrt{3}}$	$\frac{1}{\sqrt{6}}$				0	0	0
$K^- \Sigma^0$					$\frac{1}{2}$	0				0		$\frac{1}{\sqrt{2}}$
$\bar{K}^0 \Sigma^-$						$\frac{1}{2}$						$\frac{1}{2}$

- 10) T. Inoue, E. Oset and M. J. Vicente Vacas, Phys. Rev. C **65** (2002), 035204.
- 11) A. Ramos, E. Oset and C. Bennhold, Phys. Rev. Lett. **89** (2002), 252001.
- 12) J. A. Oller and U. G. Meissner, Phys. Lett. B **500** (2001), 263.
- 13) C. Garcia-Recio, M. F. M. Lutz and J. Nieves, Phys. Lett. B **582** (2004), 49.
- 14) D. Jido, J. A. Oller, E. Oset, A. Ramos and U. G. Meissner, Nucl. Phys. A **725** (2003), 181.

Table XII. $A_{ij}^d(S = -1, Q = 0)$

	$K^- p$	$\bar{K}^0 n$	$\pi^0 \Lambda$	$\pi^0 \Sigma^0$	$\eta \Lambda$	$\eta \Sigma^0$	$\pi^+ \Sigma^-$	$\pi^- \Sigma^+$	$K^+ \Xi^-$	$K^0 \Xi^0$
$K^- p$	1	$\frac{1}{2}$	$-\frac{\sqrt{3}}{8}$	$\frac{3}{8}$	$-\frac{1}{24}$	$\frac{1}{8\sqrt{3}}$	0	$\frac{3}{4}$	0	0
$\bar{K}^0 n$		1	$\frac{\sqrt{3}}{8}$	$\frac{3}{8}$	$-\frac{1}{24}$	$-\frac{1}{8\sqrt{3}}$	$\frac{3}{4}$	0	0	0
$\pi^0 \Lambda$			$\frac{2}{3}$	0	0	$\frac{2}{3}$	0	0	$-\frac{\sqrt{3}}{8}$	$\frac{\sqrt{3}}{8}$
$\pi^0 \Sigma^0$				2	$\frac{2}{3}$	0	0	0	$\frac{3}{8}$	$\frac{3}{8}$
$\eta \Lambda$					$\frac{1}{9}$	0	$\frac{2}{3}$	$\frac{2}{3}$	$-\frac{1}{24}$	$-\frac{1}{24}$
$\eta \Sigma^0$						$\frac{2}{3}$	0	0	$\frac{1}{8\sqrt{3}}$	$-\frac{1}{8\sqrt{3}}$
$\pi^+ \Sigma^-$							2	0	$\frac{3}{4}$	0
$\pi^- \Sigma^+$								2	0	$\frac{3}{4}$
$K^+ \Xi^-$									1	$\frac{1}{2}$
$K^0 \Xi^0$										1

Table XIII. $A_{ij}^f(S = -1, Q = 0)$

	$K^- p$	$\bar{K}^0 n$	$\pi^0 \Lambda$	$\pi^0 \Sigma^0$	$\eta \Lambda$	$\eta \Sigma^0$	$\pi^+ \Sigma^-$	$\pi^- \Sigma^+$	$K^+ \Xi^-$	$K^0 \Xi^0$
$K^- p$	0	$\frac{1}{2}$	$-\frac{3\sqrt{3}}{8}$	$-\frac{3}{8}$	$-\frac{1}{8}$	$-\frac{1}{8\sqrt{3}}$	0	$-\frac{3}{4}$	0	0
$\bar{K}^0 n$		0	$\frac{3\sqrt{3}}{8}$	$-\frac{3}{8}$	$-\frac{1}{8}$	$\frac{1}{8\sqrt{3}}$	$-\frac{3}{4}$	0	0	0
$\pi^0 \Lambda$			0	0	0	0	0	0	$\frac{3\sqrt{3}}{8}$	$-\frac{3\sqrt{3}}{8}$
$\pi^0 \Sigma^0$				0	0	0	0	0	$\frac{3\sqrt{3}}{8}$	$-\frac{3\sqrt{3}}{8}$
$\eta \Lambda$					0	0	0	0	$\frac{1}{8}$	$\frac{1}{8}$
$\eta \Sigma^0$						0	$\frac{2}{\sqrt{3}}$	$-\frac{2}{\sqrt{3}}$	$\frac{1}{8\sqrt{3}}$	$-\frac{1}{8\sqrt{3}}$
$\pi^+ \Sigma^-$							0	0	$\frac{3}{4}$	0
$\pi^- \Sigma^+$								0	0	$\frac{3}{4}$
$K^+ \Xi^-$									0	$-\frac{1}{2}$
$K^0 \Xi^0$										0

- 15) T. Hyodo, S. I. Nam, D. Jido and A. Hosaka, Phys. Rev. C **68** (2003), 018201.
- 16) E. E. Kolomeitsev and M. F. M. Lutz, Phys. Lett. B **585** (2004), 243.
- 17) M. F. M. Lutz and E. E. Kolomeitsev, in Proc. of *28th Int. Workshop on Gross Properties of Nuclei and Nuclear Excitations: Hadrons in Dense Matter*, Hirschegg, Austria, 16-22 January 2000; nucl-th/0004021.
- 18) D. Jido, E. Oset and A. Ramos, Phys. Rev. C **66** (2002), 055203.
- 19) A. Gomez Nicola, J. Nieves, J. R. Pelaez and E. Ruiz Arriola, Phys. Lett. B **486** (2000), 77.
- 20) G. F. Chew and S. Mandelstam, Phys. Rev. **119** (1960), 467.
- 21) U.-G. Meissner and J. A. Oller, Nucl. Phys. A **673** (2000), 311.
- 22) For example, J. F. Donoghue, E. Golowich, and B. R. Holstein, *Dynamics of the standard model* (Cambridge University Press, London, 1992).
- 23) R. J. Nowak *et al.*, Nucl. Phys. B **139** (1978), 61.
- 24) D. N. Tovee *et al.*, Nucl. Phys. B **33** (1971), 493.
- 25) T. S. Mast *et al.*, Phys. Rev. D **14** (1976), 13.
- 26) J. Ciborowski *et al.*, J. of Phys. **G8** (1982), 13.
- 27) R. O. Bangerter *et al.*, Phys. Rev. D **23** (1981), 1484.
- 28) T. S. Mast *et al.*, Phys. Rev. D **11** (1975), 3078.
- 29) M. Sakitt *et al.*, Phys. Rev. **139** (1965), B719.
- 30) M. B. Watson, M. Ferro-Luzzi and R. D. Tripp, Phys. Rev. **131** (1963), 2248.
- 31) J. K. Kim, Phys. Rev. Lett. **14** (1965), 29.
- 32) M. Ferro-Luzzi, R. D. Tripp and M. B. Watson, Phys. Rev. Lett. **8** (1962), 28.
- 33) M. Csejthe-Barth *et al.*, Phys. Lett. **16** (1965), 89.
- 34) J. Paul Nordin, Phys. Rev. **123** (1961), 2168.
- 35) W. Kittel, G. Ptter, and I. Wacek, Phys. Lett. **21** (1966), 349.
- 36) H. Going, Nuovo Cim. **16** (1960), 848.

Table XIV. $B_{ij}^d(S = -1, Q = 0)$

	$K^- p$	$\bar{K}^0 n$	$\pi^0 \Lambda$	$\pi^0 \Sigma^0$	$\eta \Lambda$	$\eta \Sigma^0$	$\pi^+ \Sigma^-$	$\pi^- \Sigma^+$	$K^+ \Xi^-$	$K^0 \Xi^0$
$K^- p$	1	$\frac{1}{2}$	$-\frac{1}{8\sqrt{3}}$	$\frac{1}{8}$	$\frac{5}{24}$	$-\frac{5}{8\sqrt{3}}$	0	$\frac{1}{4}$	0	0
$\bar{K}^0 n$		1	$\frac{1}{8\sqrt{3}}$	$\frac{1}{8}$	$\frac{5}{24}$	$\frac{5}{8\sqrt{3}}$	$\frac{1}{4}$	0	0	0
$\pi^0 \Lambda$		0	0	0	0	0	0	$-\frac{1}{8\sqrt{3}}$	$\frac{1}{8\sqrt{3}}$	
$\pi^0 \Sigma^0$			0	0	0	0	0	$\frac{1}{8}$	$\frac{1}{8}$	
$\eta \Lambda$					$\frac{16}{9}$	0	0	0	$\frac{5}{24}$	$\frac{5}{24}$
$\eta \Sigma^0$						0	0	0	$-\frac{5}{8\sqrt{3}}$	$\frac{5}{8\sqrt{3}}$
$\pi^+ \Sigma^-$							0	0	$\frac{1}{4}$	0
$\pi^- \Sigma^+$								0	0	$\frac{1}{4}$
$K^+ \Xi^-$									1	$\frac{1}{2}$
$K^0 \Xi^0$										1

Table XV. $B_{ij}^f(S = -1, Q = 0)$

	$K^- p$	$\bar{K}^0 n$	$\pi^0 \Lambda$	$\pi^0 \Sigma^0$	$\eta \Lambda$	$\eta \Sigma^0$	$\pi^+ \Sigma^-$	$\pi^- \Sigma^+$	$K^+ \Xi^-$	$K^0 \Xi^0$
$K^- p$	0	$\frac{1}{2}$	$-\frac{\sqrt{3}}{8}$	$-\frac{1}{8}$	$\frac{5}{8}$	$\frac{5}{8\sqrt{3}}$	0	$-\frac{1}{4}$	0	0
$\bar{K}^0 n$		0	$\frac{\sqrt{3}}{8}$	$-\frac{1}{8}$	$\frac{5}{8}$	$-\frac{5}{8\sqrt{3}}$	$-\frac{1}{4}$	0	0	0
$\pi^0 \Lambda$		0	0	0	0	0	0	0	$\frac{\sqrt{3}}{8}$	$-\frac{\sqrt{3}}{8}$
$\pi^0 \Sigma^0$			0	0	0	0	0	0	$\frac{1}{8}$	$\frac{1}{8}$
$\eta \Lambda$					0	0	0	0	$-\frac{5}{8}$	$-\frac{5}{8}$
$\eta \Sigma^0$						0	0	0	$-\frac{5}{8\sqrt{3}}$	$\frac{5}{8\sqrt{3}}$
$\pi^+ \Sigma^-$							0	0	$\frac{1}{4}$	0
$\pi^- \Sigma^+$								0	0	$\frac{1}{4}$
$K^+ \Xi^-$									0	$-\frac{1}{2}$
$K^0 \Xi^0$										0

37) Rutherford-London, G. P. Gopal *et al.*, Nucl. Phys. B **119** (1977), 362.
 38) R. J. Hemingway, Nucl. Phys. B **253** (1985), 742.
 39) M. Batinic, I. Slaus, A. Svarc and B. M. K. Nefkens, Phys. Rev. C **51** (1995), 2310.
 40) J. C. Hart *et al.*, Nucl. Phys. B **166** (1990), 73.
 41) D. H. Saxon *et al.*, Nucl. Phys. B **162** (1980), 522.
 42) R. D. Baker *et al.*, Nucl. Phys. B **145** (1978), 402.
 43) R. D. Baker *et al.*, Nucl. Phys. B **141** (1978), 29.
 44) B. Nelson *et al.*, Phys. Rev. Lett. **31** (1973), 901.
 45) D. W. Thomas, A. Engler, H. E. Fisk and R. W. Kraemer, Nucl. Phys. B **56** (1973), 15.
 46) J. J. Jones *et al.*, Phys. Rev. Lett. **26** (1971), 860.
 47) T. O. Binford *et al.*, Phys. Rev. **183** (1969), 1134.
 48) O. Van Dyck *et al.*, Phys. Rev. Lett. **23** (1969), 50.
 49) T. M. Knasel *et al.*, Phys. Rev. D **11** (1975), 1.
 50) R. L. Crolius *et al.*, Phys. Rev. **155** (1967), 1455.
 51) J. Keren, Phys. Rev. **133** (1963), B457.
 52) L. L. Yoder, C. T. Coffin, D. I. Meyer and K. M. Terwilliger, Phys. Rev. **132** (1963), 1778.
 53) L. B. Leipuner and R. K. Adair, Phys. Rev. **109** (1958), 1358.
 54) L. Bertanza *et al.*, Phys. Rev. Lett. **8** (1962), 332.
 55) F. S. Crawford *et al.*, Phys. Rev. Lett. **3** (1959), 394.
 56) R. T. V. de Walle, C. L. A. Pols, D. J. Schotanus, H. J. G. M. Tiecke and D. Z. Toet, Nuovo Cim. A **53** (1968), 745.
 57) O. Goussu *et al.*, Nuovo Cim. **42A** (1966), 606.
 58) F. Eisler *et al.*, Nuovo Cim. **10** (1958), 468.
 59) Center of Nuclear Study, <http://gwdac.phys.gwu.edu> .
 60) M. Gell-Mann, R. J. Oakes and B. Renner, Phys. Rev. **175** (1968), 2195.
 61) M. Gell-Mann, Phys. Rev. **125** (1962), 1067.

- 62) S. Okubo, *Prog. Theor. Phys.* **27** (1962), 949.
- 63) V. Bernard, N. Kaiser and U. G. Meissner, *Phys. Lett. B* **309** (1993), 421.
- 64) V. Bernard, N. Kaiser and U. G. Meissner, *Phys. Rev. C* **52** (1995), 2185.
- 65) V. Bernard, N. Kaiser and U.-G. Meissner, *Int. J. Mod. Phys. E* **4** (1995), 193.
- 66) G. Ecker, J. Gasser, A. Pich and E. de Rafael, *Nucl. Phys. B* **321** (1989), 311.
- 67) P. J. Fink, G. He, R. H. Landau and J. W. Schnick, *Phys. Rev. C* **41** (1990), 2720.
- 68) D. Jido, A. Hosaka, J. C. Nacher, E. Oset and A. Ramos, *Phys. Rev. C* **66** (2002), 025203.
- 69) C. Garcia-Recio, J. Nieves, E. Ruiz Arriola, and M. J. Vicente Vacas, *Phys. Rev. D* **67** (2003), 076009.
- 70) S. I. Nam, H. -Ch. Kim, T. Hyodo, D. Jido and A. Hosaka, [hep-ph/0309017](#).
- 71) T. Hyodo, A. Hosaka, E. Oset, A. Ramos and M. J. Vicente Vacas, *Phys. Rev. C* **68** (2003), 065203.
- 72) T. Hyodo, A. Hosaka, M. J. V. Vacas and E. Oset, *Phys. Lett. B* **593** (2004), 75.
- 73) C. Bennhold and H. Tanabe, *Nucl. Phys. A* **530** (1991), 625.
- 74) M. Gell-Mann, *Phys. Rev.* **92** (1954), 833.
- 75) T. Nakano and K. Nishijima, *Prog. Theor. Phys.* **10** (1954), 581.